International Journal of Mechanical, Industrial and Aerospace Sciences
ISSN: 2517-9950
Vol:9, No:11, 2015

A Fault Analysis Cracked-Rotor-to-Stator Rub and Unbalance by Vibration Analysis Technique

B. X. Tchomeni, A. A. Alugongo, L. M. Masu

***Abstract*—**An analytical 4-DOF nonlinear model of a de Laval rotor-stator system based on Energy Principles has been used theoretically and experimentally to investigate fault symptoms in a rotating system. The faults, namely rotor-stator-rub, crack and unbalance are modeled as excitations on the rotor shaft. Mayes steering function is used to simulate the breathing behaviour of the crack. The fault analysis technique is based on waveform signal, orbits and Fast Fourier Transform (FFT) derived from simulated and real measured signals. Simulated and experimental results manifest considerable mutual resemblance of elliptic-shaped orbits and FFT for a same range of test data.

***Keywords*—**A breathing crack, fault, FFT, nonlinear, orbit, rotor-stator rub, vibration analysis.

I. Introduction

DESIGN and vibration control of rotating machines require prediction of dynamic characteristics; resonance thresholds, stability limits, participating modes and interactions of machine parts in the sub-critical and in super-critical regimes [1]. Rotor-stator rub involves several phenomena; impact, friction, and stiffness modification among others. Rub forces significantly affect system's stability limits [2].

A rotor-stator rub diagnostic model and experimentally dynamic characteristics were reported in [3]. This model has gained a wide application to-date.

A model of torsional-lateral vibrations with rotor-to-stator rub was proposed in [4]. Rub was simulated as elastic impact-contact, and rub forces represented by friction coefficient, normal and tangential forces at rotor-stator contact point. The system response orbits show clearly the rotor-to-stator impact contact in the start-up period.

A multi-mass model to assess the degree to which chaos is distributed in a rotor- stator system was developed in [5].

An analysis of rotor-stator rub done on system bifurcation using various damping ratios, Poincare map and FFT spectrum in [6] revealed predominance of rub at the bottom of the clearance circle at a low rotor speed. A quasi-periodic model of a rotor with a bearing clearance using Harmonic Balance Method has been reported in [7]. A subsequent stability analysis revealed system's nonlinear features.

Rotor-stator rub was modeled and stiffening of rotor shaft quantitatively investigated in [8]. Change in transient stiffness served as a sufficient indicator of rub-impact.

Rotor-stator rubs and the often-neglected axial force effect in a Lagrangian formulation were analyzed by FFT [9]. Simulation at a constant shaft speed failed to indicate most of the nonlinear phenomena. At non-uniform speed, nonlinear features including bifurcation and chaos were observed.

The vibration behavior of unbalanced rotating shaft while passing via critical speed has significant interest in detecting malfunction of rotating machines. The unbalance may occur due to factors such as rotor fatigue crack.

Gash considered the non-stationary mechanism of a closing crack with various flexibilities for open and closed cracks [10]. While Grabowski suggested that non-linearity does not affect the crack, response since the cracks opens and closes continually with the rotation [11].

Recently, several authors have shown interest in accelerating cracked rotor dynamics. Analysis of the cracked shafts vibration focuses on, acceleration or deceleration phases of the shaft, passage via the critical speed and coupling between diverse vibrations modes [12]. In [13], a detailed analytical and experimental investigation on a cracked shaft was reported. The open-closure behavior of a transversal crack was simulated by a cosine function.

Thematic analysis presented in the current work concerns the understanding of complex coupled dynamics of unbalanced rotors, and the intermittent interaction of the rotor-stator in presence of transverse crack.

Experimental data for the investigation is obtained by measurements taken on RK-4 rotor kit. The crack simulators two radial orthogonal springs were used. An eccentric mass and a screw were used to induce unbalance and rotor-stator rub respectively. In this analysis, the model in [4], [9] is adopted. The basic system layout is shown in Figs. 1-3.

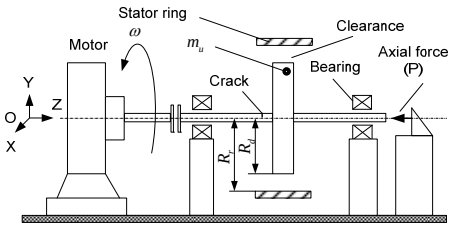

Fig. 1 Motor-shaft-disc –stator-transverse crack and axial force

B. X. Tchomeni, postgraduate student is with the Mech. Eng Dept., Vaal University of Technology, Andries Potgieter 1900, Vanderbijlpark, RSA (Phone: +27- 169509302; fax: +27-169509797; e-mail: bmignon@gmail.com).

A. A. Alugongo, is with the Mech. Eng. Dept., Vaal University of Technology, Andries Potgieter 1900, Vanderbijlpark, RSA (Phone: +27-169509302; fax: +27-169509797; e-mail:alfayoa@vut.ac.za).

L. M. Masu, is with the Mech. Eng Dept., Vaal University of Technology, Andries Potgieter 1900, Vanderbijlpark, RSA (Phone: +27- 169506817; fax: +27-169509797;e-mail:leonard@vut.ac.za).

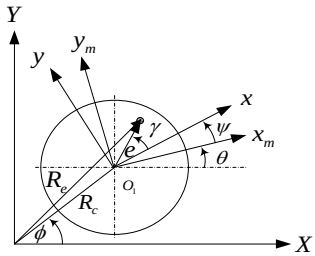

Fig. 2 Section view of disc on the shaft in inertial, rotating and motor coordinates (X, Y), (x, y), (x_m, y_m) respectively

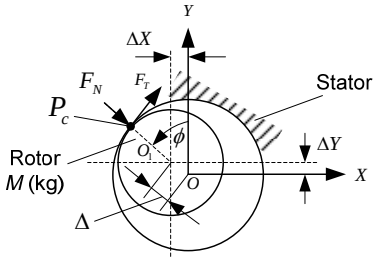

Fig. 3 Geometry of rotor, rubbing impact forces and a clearance

II. Forces Acting on the Rotor's Shaft

Applying the approach in [14] to Fig. 3, the positions of shaft center and rotor-stator clearance are:

$$\vec{R} = X\vec{\imath} + Y\vec{\jmath} \tag{1}$$

and

$$\Delta = R_r - R_s. \tag{2}$$

Friction forceF_T, acts at the contact point. Contact occurs when,

$$R - \Delta \geq 0 \tag{3}$$

When $R < \Delta$, contact ceases and F_T vanishes. Therefore,

$$F_N = K_s(R - \Delta); \quad F_T = -\mu K_s(R - \Delta) \tag{4}$$

$F_N$and μ respectively are, radial component due to impact and friction coefficient. Lateral forces in $X$and Y directions are:

$$F_X = -F_N cos\emptyset + F_T sin\emptyset;\ F_Y = -F_N sin\emptyset - F_T cos\emptyset \tag{5}$$

In Cartesian coordinates, the forces are expressed as,

$$F_X = -K_s\left(1 - \frac{\Delta}{R}\right)X + K_s\left(1 - \frac{\Delta}{R}\right)\mu Y \tag{6}$$

$$F_Y = -K_s\left(1 - \frac{\Delta}{R}\right)\mu X - K_s\left(1 - \frac{\Delta}{R}\right)Y \tag{7}$$

III. Potential Energy Expression

The system elastic strain energy is:

$$V = \frac{1}{2}K_{XX}X^2 + \frac{1}{2}K_{YY}Y^2 + \frac{1}{2}K_{\psi\psi}\psi^2 \tag{8}$$

A high rotor speed the bending stiffness as given in [9].

$$K_{XX} = K_{YY} = K_b - \frac{P\pi^2}{2L} - \frac{F_\psi \pi^3}{2L^2}; \tag{9}$$

K_b, P and $F_\psi$are correspondingly, first modal stiffness in bending mode, fluctuating axial force and axial torque. In this paper P and F_ψ are prescribed a priori as in [15].

$$P = 0,\ F_\psi = 0 \tag{10}$$

IV. Unbalanced Rotor-Stator System

Considering Kinetic energy, Rayleigh Dissipation function and Strain energy in, Figs. 1-3, the dynamic equation linking the physical parameters of the system model is [4]:

$$\begin{bmatrix} m_{\theta\theta} & m_{\theta\psi} & m_{\theta X} & m_{\theta Y} \\ m_{\psi\theta} & m_{\psi\psi} & m_{\psi X} & m_{\psi Y} \\ m_{X\theta} & m_{X\psi} & m_{XX} & 0 \\ m_{Y\theta} & m_{Y\psi} & 0 & m_{YY} \end{bmatrix} \begin{Bmatrix} \ddot{\theta} \\ \ddot{\psi} \\ \ddot{X} \\ \ddot{Y} \end{Bmatrix} + \begin{bmatrix} 0 & 0 & 0 & 0 \\ 0 & C_{\psi\psi} & 0 & 0 \\ 0 & 0 & C_{XX} & C_{XY} \\ 0 & 0 & C_{YX} & C_{YY} \end{bmatrix} \begin{Bmatrix} \dot{\theta} \\ \dot{\psi} \\ \dot{X} \\ \dot{Y} \end{Bmatrix} + \begin{bmatrix} 0 & 0 & 0 & 0 \\ 0 & K_{\psi\psi} & 0 & 0 \\ 0 & 0 & K_{XX} & K_{XY} \\ 0 & 0 & K_{YX} & K_{YY} \end{bmatrix} \begin{Bmatrix} \theta \\ \psi \\ X \\ Y \end{Bmatrix} + \begin{Bmatrix} Q_\theta \\ 0 \\ Q_X \\ Q_Y \end{Bmatrix} = \begin{Bmatrix} F_\theta \\ F_\psi \\ F_X \\ F_Y \end{Bmatrix} \tag{11}$$

The parameters of (11) are obtained from [14].

V. A Cracked Rotor-Stator System

A hinge mechanism is incorporated in the shaft to provide for local flexibility of a breathing crack [10]. Shear stresses are discarded, Saint-Venant's principle observed [16], manipulation as in [13] performed on (11) resulting in the dynamic equation of the cracked-rotor-rub system [14]:

$$\begin{bmatrix} m_{\theta\theta} & m_{\theta\psi} & m_{\theta X} & m_{\theta Y} \\ m_{\psi\theta} & m_{\psi\psi} & m_{\psi X} & m_{\psi Y} \\ m_{X\theta} & m_{X\psi} & m_{XX} & 0 \\ m_{Y\theta} & m_{Y\psi} & 0 & m_{YY} \end{bmatrix} \begin{Bmatrix} \ddot{\theta} \\ \ddot{\psi} \\ \ddot{X} \\ \ddot{Y} \end{Bmatrix} + \begin{bmatrix} 0 & 0 & 0 & 0 \\ 0 & C_{\psi\psi} & 0 & 0 \\ 0 & 0 & C_{XX} & C_{XY} \\ 0 & 0 & C_{YX} & C_{YY} \end{bmatrix} \begin{Bmatrix} \dot{\theta} \\ \dot{\psi} \\ \dot{X} \\ \dot{Y} \end{Bmatrix} + \begin{bmatrix} 0 & 0 & 0 & 0 \\ 0 & K_{\psi\psi} & 0 & 0 \\ 0 & 0 & K_{XX} & K_{XY} \\ 0 & 0 & K_{YX} & K_{YY} \end{bmatrix} \begin{Bmatrix} \theta \\ \psi \\ X \\ Y \end{Bmatrix} + \frac{1}{2}f(t)\Delta k_{xx} \times \begin{bmatrix} 0 & 0 & 0 & 0 \\ 0 & 0 & 0 & 0 \\ 0 & 0 & 1 - cos2\theta & sin2\theta \\ 0 & 0 & sin2\theta & 1 + cos2\theta \end{bmatrix} \begin{Bmatrix} 0 \\ 0 \\ 0 \\ Ys \end{Bmatrix} = \begin{Bmatrix} Q_\theta \\ 0 \\ Q_X \\ Q_Y \end{Bmatrix} + \begin{Bmatrix} F_\theta \\ F_\psi \\ F_X \\ F_Y \end{Bmatrix} \tag{12}$$

Δk_{xx},K_0, and $f(\theta)$ are respectively, change in stiffness in the weaker axis due to the crack, uncracked shaft stiffness and steering function. $f(\theta)$is taken from [13].

VI. Experimental Set-Up

The experimental equipment used is shown in Figs. 4 and 5. Fig. 4 shows the setup that adopted. The rig comprises a motor speed control, proximity probes and data acquisition interface unit that is controlled by Ascent and Matlab toolbox. In the mounting blocks, probes were used to measure the displacement of the rotor shaft at various positions. All the outputs were displayed an oscillator with filter analysis. The rotor was set up on a rigid base to avoid disturbances that could influence the measurements.

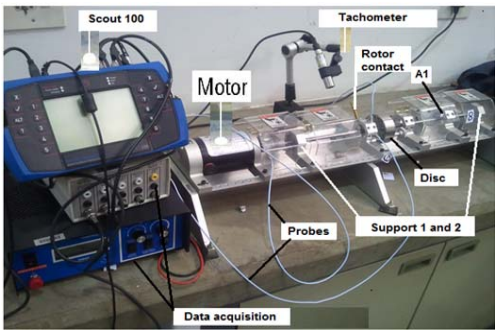

Fig. 4 Experimental set-up for fault detection in a rotor with data acquisition

The test rig comprises an elastic shaft and one rigid disc. The rotor was driven by a motor a shaft through a flexible coupling.

The shaft was supported on two roller bearings at both ends and sustained by two fixed steel supports (designated by Support1 and *2* in Fig. 4). The shaft length and diameter were 570 mm and 10mm respectively. The disc of inside diameter 10 mm, outside diameter 75 mm and thickness 25 mm with a mass 0.845kg were mounted at a position 290 mm from the right end of the rotor. Unbalance was achieved by adjusting a small mass $m = 0.018kg$ at one point of on the disc 10 mm from the shaft circumference.

The sensors recorded acceleration of the shaft in the three directions (Fig. 5).

The vibrations in the axial direction did not provide information on the presence of a crack; its data will not be presented hereafter.

The rotor's crack was positioned 240mm from the left hand side by mounting a crack simulator and two orthogonal springs. Thus, the system under consideration has the faults, 'breathing' crack, unbalance and rub.

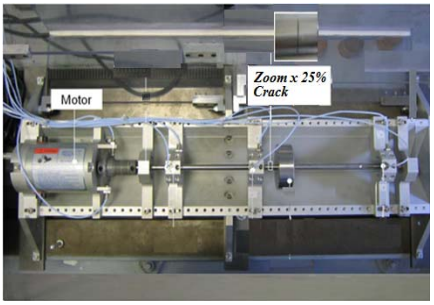

Fig. 5 Test rig setup for shaft rotation measurement with crack

The RK-4 Rotor Kit motor could closely hold the desired speed with changes in loading conditions. The motor was run counter-clockwise and had at a slow speed. The motor was set to run at a maximum speed fixed at 4500 rpm by using the motor speed control. The shaft acceleration was controlled by laser tachometer. The vibration measurements of the shaft were captured by four proximity probes, wherein, two probes were meant for relative shaft displacement measurements, and the other two probes were for Keyphasor (one-per-turn) phase reference pulse generation and for Motor Speed Control speed sensing.

Rotor-stator rub was realized at point (A1) by introducing a small tight screw at a favorable distance between the rotor and the stator. Continuous slightest contact could occur during the rotation of the shaft and was recorded by the proximity probes.

The probes consisted of two orthogonal sensors and were placed at 210 mm from plane A1 near the left and right supports at proximity of the rotor-stator contact and crack's position. The probes were positioned at distances sufficient to detect the vibrations of the shaft and avoid any contact that could occur between the tip of the probe and a portion of the revolving assembly under conditions of extreme vibration. To measure the relative displacement of the shaft; two mutually perpendicular proximity probes were mounted at ± 90 ° from the true vertical and oriented in two planes perpendicular to the shaft. The probes must be staggered in the probe block probe (Fig. 6). The vertical and horizontal probe went respectively to Probe #1 and Probe #2 input of the RK4 Proximitor Assembly.

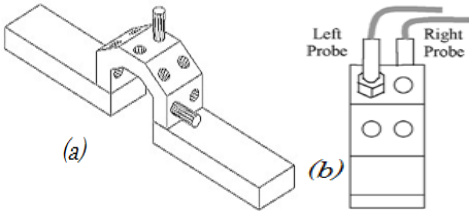

Fig. 6 Schematic of the proximity probes, (a) viewed from the drive and (b) viewed from the left side

The data analysis software was Commtest instrument version 11.6.0 for Bently Nevada™ combined with ASCENT 2013 that linked together with a SCOUT100 Data Acquisition Interface Unit (DAIU) used in this experimental setup.

Commtest instrument for ASCENT software is specifically designed for capturing machinery data. This system is extremely versatile, incorporating the properties and capabilities of oscilloscopes, spectrum analyzers, filters, and recording instruments. SCOUT100 DAIU is a processing unit and interfaces directly to a computer. Two proximity probes for relative shaft displacement measurements and a Keyphasor® probe were connected to the SCOUT100 DAIU inputs through a Proximitor® assembly (Fig. 4).

The main objective of this experiment was to diagnose using relative shaft displacement approach, the fault on rotors through transient signal and afterward, analyze the corresponding signal with those obtained in three degree of freedom simulation.

VII. Numerical Simulation, Experimental Results and Discussion

To investigate excitations induced by the external forces, the system parameters in [4] are adopted for simulation. Two investigations are performed, the first is the numerical

simulation of (12) on diverse hypothesis by a Modified Runge-Kutta algorithm in MATLAB giving X, Y, θ at a time step $\Delta_t = 0.001s$, between $t = 0$s and $t = 20\,s$. The rotor response with and without external forces, obtained during start-up of the rotor are then presented and discussed.

The second is the experimental study of the model, where the system DOF is lumped on the disc as two orthogonal lateral deflections of the disc's geometrical center and one rigid-body rotation.

In the set of experiments, analysis is carried out first in absence of external excitation forces. The rotor dynamic characteristics are determined from the vibration measurements. In the second set of experiments, the rubbing contact clearance is put in place and measurements are taken for the excitations forces condition.

In experimental analysis, the motor torque is designed to rotate the rotor system to an angular velocity 5000 r.p.m (not exceeding operational limits of the bearings).

Signal measurements were based on long time Waveform experimental data. The after acquisition, the data was transferred to a PC and analysis of performed on time waveform, frequency spectrum and orbit. Resultant plots gave the amplitude of vibration of the system as viewed from the associated proximity probe.

The R-K4 was set to run counter-clockwise and its speed fixed in interval [900 - 4500 rpm] by motor speed control. The radial clearance set to a small value, and the frequency sampled at $f_s = 500Hz$.

The experimental model set up of the rotor RK-4 accounts only for the rotor lateral deflections, X, Y and rigid-body rotation θ, where the torsional D.O.F is eliminated.

Measurements at various speeds enabled visualization of evolution of the orbits and the amplitudes of harmonics based on the frequency. For convenience, the axial forces have not been taken into consideration in the entire experimental work.

VIII. Lateral Motion and Axial Forces Effects

In the first simulation the torsional deflections effect ψ is neglected. The variable stiffness can be assumed to be same as dynamic stiffness and the cracked shaft stiffness is taken into consideration. The dynamic response of the rotor passing through the critical speed without and with a crack in lateral deflections X, Y and rigid rotation θ are considered.

Equation (12) can thus be transferred into:

$$\begin{bmatrix} m_{\theta\theta} & m_{\theta X} & m_{\theta Y} \\ m_{X\theta} & m_{XX} & 0 \\ m_{Y\theta} & 0 & m_{YY} \end{bmatrix} \begin{Bmatrix} \ddot{\theta} \\ \ddot{X} \\ \ddot{Y} \end{Bmatrix} + \begin{bmatrix} 0 & 0 & 0 \\ 0 & C_{XX} & 0 \\ 0 & 0 & C_{YY} \end{bmatrix} \begin{Bmatrix} \dot{\theta} \\ \dot{X} \\ \dot{Y} \end{Bmatrix} + \begin{bmatrix} 0 & 0 & 0 \\ 0 & K_{XX} & 0 \\ 0 & 0 & K_{YY} \end{bmatrix} \begin{Bmatrix} \theta \\ X \\ Y \end{Bmatrix} = \frac{1}{2} f(t) \Delta k_{xx} \begin{bmatrix} 0 & 0 & 0 \\ 0 & 1 - cos2\theta & sin2\theta \\ 0 & sin2\theta & 1 + cos2\theta \end{bmatrix} \begin{Bmatrix} 0 \\ 0 \\ Y_{st} \end{Bmatrix} - \begin{Bmatrix} Q_\theta \\ Q_X \\ Q_Y \end{Bmatrix} + \begin{Bmatrix} T_f \\ 0 \\ 0 \end{Bmatrix} \quad (13)$$

X,Y and θ are evaluated on passing via critical speed with and without a crack. Cross-coupling stiffness and damping coefficients adopted are, $C_{XY} = C_{YX} = K_{XY} = K_{YX} = 0$.

Time and frequency-domain response are obtained numerically by integrating (13) by a modified Runge–Kutta algorithm, at a high speed up to $10000\ r.p.m$.

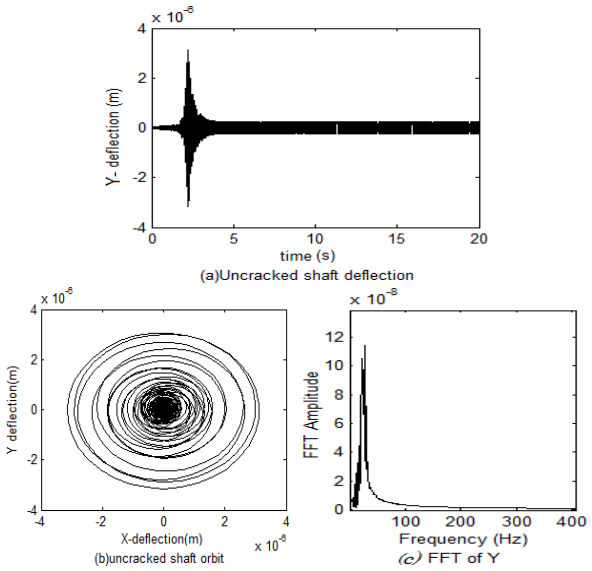

Fig. 7 Dynamic response, no torsional flexibility, rub, crack but axial force, $\Delta K_\xi/K_b$=0, ψ =0, P=2kN: (a) Vertical deflection of uncracked shaft; (b) Rotor response orbit; (c) Y-lateral frequency

Figs. 7 and 8 illustrate the unbalanced response of the rotor in case of no crack and rub condition.

Comparing the orbits in Figs. 7 and 8, it is apparent that, the unbalance is a source of extra evolution in the vibration response, especially when the rotating speed falls in the neighborhood of half of the system critical speed.

It is observed that the presence of unbalanced induced a closed-loop containing a circular loop inside. As obtained in Figs. 7 (b) and 8 (b) the orbit first varied from the minimum response at the start-up to the maximum response $R = 23.3mm$ at the resonance and went back in a regular closed inside loop.

The maximum orbit amplitudes in Fig. 7 (b) are modified from $R_1 = 3.167 \times 10^{-6}m$ to $R_2 = 2{,}3 \times 10^{-4}m$ in Fig. 8 (b) when the critical speed changes respectively from $\omega_1 = 1132.27\ rpm$ in Fig. 7 (c) to $\omega_2 = 1124.43\ rpm$ in Fig. 8 (c). i.e from a simulated to the experiment unbalanced shaft. In Fig. 8 (c), the frequency amplitudes of the experiment is greater than that of a simulated rotor with small axial force in Fig. 7 (c). FFT analysis in Fig. 8 (c) reveals that a high vibrational level is reached by order 1 harmonic at $23.46\ Hz$. Numerous peaks are observed when the rotor speeds via its first critical speed $\dot{\theta} = 1124\ rpm$. The FFT plot also shows that the higher frequencies for example 1X, get excited due to the load and sub-harmonics at 1/2X, arise due to the unbalance.

From the vertical deflection time wave in Fig. 8 (a), the first critical speed is observed in both cases at different times corresponding to the critical speed $\omega_1$and ω_2. It is observed that, unbalanced shaft is characterized by presence of regular circular loops with presence of higher frequency 1X due to the unbalanced load. The simulated and experimental results obtained at high speed (Fig. 7) are resembled in deflection shapes, frequencies and orbits amplitude.

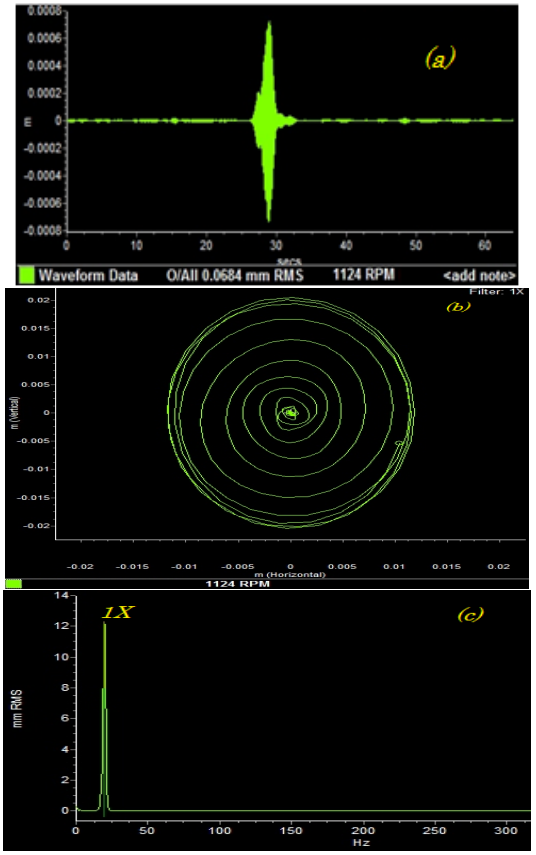

Fig. 8 Dynamics rotor system response with extra mass at high speed 1124 rpm. (a) Lateral unbalanced shaft deflection (b) Rotor response orbit, (c) Frequency signal domain

XVI. Pertubation Effect of Rotor-Stator Rubbing

The presence of the unbalance and reduction of clearance generate a larger rotor-stator frictional force at each impact. It is necessary to analyze the evolution of this phenomenon with motor speed. The previous simulations and experiments are repeated at various speeds. The equation of interaction between rotor-stator and opening and closing crack are re-written as:

$$\begin{bmatrix} m_{\theta\theta} & m_{\theta X} & m_{\theta Y} \\ m_{X\theta} & m_{XX} & 0 \\ m_{Y\theta} & 0 & m_{YY} \end{bmatrix} \begin{Bmatrix} \ddot{\theta} \\ \ddot{X} \\ \ddot{Y} \end{Bmatrix} + \begin{bmatrix} 0 & 0 & 0 \\ 0 & C_{XX} & 0 \\ 0 & 0 & C_{YY} \end{bmatrix} \begin{Bmatrix} \dot{\theta} \\ \dot{X} \\ \dot{Y} \end{Bmatrix} + \begin{bmatrix} 0 & 0 & 0 \\ 0 & K_{XX} & 0 \\ 0 & 0 & K_{YY} \end{bmatrix} \begin{Bmatrix} \theta \\ X \\ Y \end{Bmatrix} = \begin{Bmatrix} Q_\theta \\ Q_X \\ Q_Y \end{Bmatrix} + \begin{Bmatrix} F_\theta \\ F_X \\ F_Y \end{Bmatrix} + \left(\frac{1}{2} f(t) \Delta k_{xx} \begin{bmatrix} 0 & 0 & 0 \\ 0 & 1-cos2\theta & sin2\theta \\ 0 & sin2\theta & 1+cos2\theta \end{bmatrix} \begin{Bmatrix} 0 \\ 0 \\ Y_{st} \end{Bmatrix} \right) \quad (14)$$

Simulation of (14) has been performed at the clearance chosen $\Delta = 1.65 \times 10^{-6} m$.

Figs. 9 and 10 highlight simulated and experimental features of the rotor under rotor-stator rub, axial force and unbalance.

Existence of considerable disparities on both time-deflections under rub was noted at a higher level of vibrations in Fig. 10 (a) where the first critical speed is observed at $t = 32s$ experimentally and $t = 3s$ by simulation. This is because contact between rotor and stator increases the rotor dynamic stiffness, and this increases the rotor critical speed.

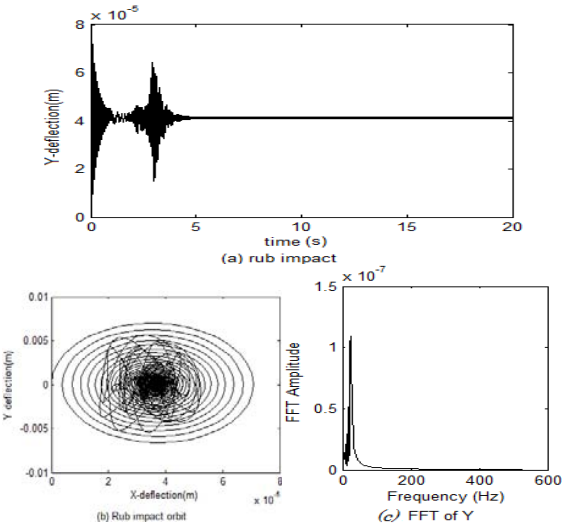

Fig. 9 Rotor lateral-rotor response without torsional deformation, with rub, axial force: $\Delta K_\xi / K_b = 0$, $\psi = 0$. P=2000N (a) Vertical uncracked shaft deflection (b) Rotor response orbit, (c) Y-Lateral frequency signal

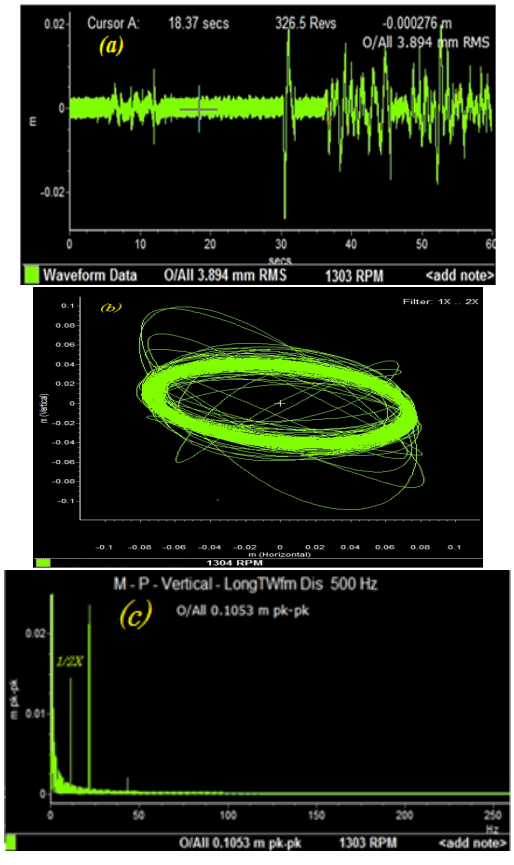

Fig. 10 Rotor system response using the lateral-rotor model at high speed 1303 rpm, with rotor-to-stator rubbing: (a) Vertical deflection (b) orbit, (c) Frequency signal domain

Fig. 9 (a) shows the synchronous lateral response of the rotor as a function of time. The critical speed of the shaft is found to be 799.6140 rpm after $t = 3s$ where large peak amplitude is observed (Fig. 9 (a)). Experimentally it appears that the contact between the rotor and the stator increases the rotor critical speed to 1303 rpm.

The presence of the unbalance and reduction of clearance generates a larger frictional force at each impact of the rotor to the stator. The amplitude of the peaks caused by defects increases with the number of contacts, this phenomenon is explained by a decrease in clearance and the increasing of a percentage solid contact.

Observation of the orbit in Fig. 9 (b)) shows complex shapes from the evolution of the contacts (rebounds) at the impact point.

As predicted in Fig. 9 (b) the experimental orbit's result indicates that, orbits are significantly distorted due to rubs into the system. The inside circular-looped orbit obtained for an unbalance is drastically modified to an outside elliptic shape characteristic of severe rubbing contact.

Spectral analysis shows that in normal operation, the contact effect creates an important component in the frequency spectrum. The occurrence of the contacts on the system modifies the spectrum by modulating the signal at the shaft rotation frequency.

The spectral analysis in (Fig. 10 (c)) exhibits an increase in the magnitude of frequency components as observed previously in Fig. 9 (c) by the appearance of squashed sub-harmonic peaks before the main peaks.

It should be noted that the tightening 1/2X … harmonics in Fig. 10 (c) which represents the sub-harmonics frequencies peaks are mainly due to unbalance and rub. In Fig. 10 (c), the main peak is well at the frequency of rotor, 22.5Hz. The gap between each peak is in the range of 22.5 Hz, which is the shaft rotation frequency.

This observation of peaks will enable to follow the evolution of a default. The severity of the rub is then a function of the number and the size of these different peaks.

The size of the inside loop and the abrupt change in orbit as the rotor passes via the first critical speed can be used as an indicator of rub fault and the bounces inside the loops can be assigned as rub signature.

XV. Detection of the Crack of the Crack-Rub with Both Simulation and Experimental Approach

The experiment is carried out for two cases: transverse crack without rub and transverse crack with severe rubbing. The solutions for the both cases are determined by using a spectral technique as in simulation.

The review of the vibration response of the rotor dynamic system with a relatively deep transverse crack ($\Delta k = \frac{\Delta}{k} \approx$ 50%), allows obtaining the orbit and the amplitude spectrum in accordance with the experimental study elaborated in Figs. 12 and 14.

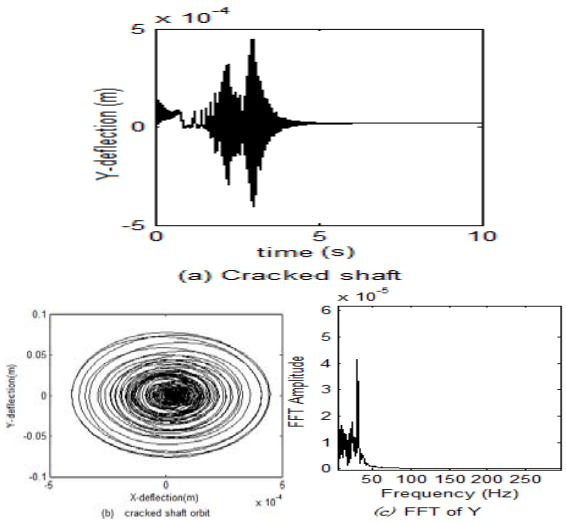

Fig. 11 Dynamic response of cracked rotor via the critical speed, with axial force, and no rub, $\Delta K_\xi/K_b$=0.542, P=2 kN, (a) Y- cracked shaft deflection; (b) Rotor response orbit; (c) Y-Lateral frequency

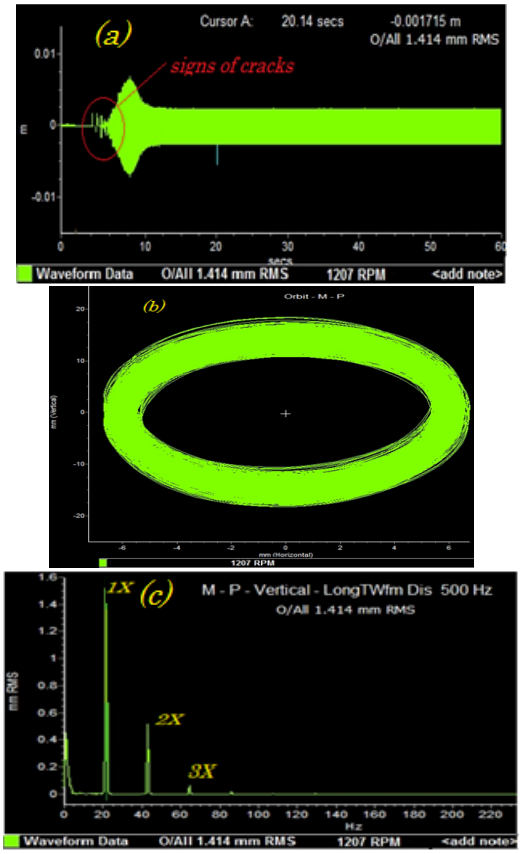

Fig. 12 Rotor system response using the lateral-rotor model at high speed 1207 rpm, with unbalance and crack ($\Delta K_\xi/K_b$=0.5). (a) Vertical deflection (b) orbit, (c) Frequency signal domain

Comparing the orbits in Figs. 11 and 7, it is apparent that, the breathing crack is a source of extra evolution in the

vibration response, especially when the rotating speed falls in the neighborhood of half of the system critical speed.

The maximum orbit amplitudes in Fig. 16 are modified from $R_1 = 3.167 \times 10^{-6} m$ to $R_2 = 5.025 \times 10^{-4} m$ when the speed changes respectively from $\omega_1 = 1132.27\, rpm$ in Fig. 7 (c) to $\omega_2 = 1855.43\, rpm$ in Fig. 11 (c) i.e. from a healthy to a cracked shaft. The cracked shaft is characterized by presence of strong tightening loops. In Fig. 12 (c), the frequency amplitudes where the inside orbit loop is higher is present, is greater than that of a rotor with small axial force in Fig. 7 (c) and 8 (c) reveals that a high vibrational level is reached by order 1 harmonic at 23.46 Hz.

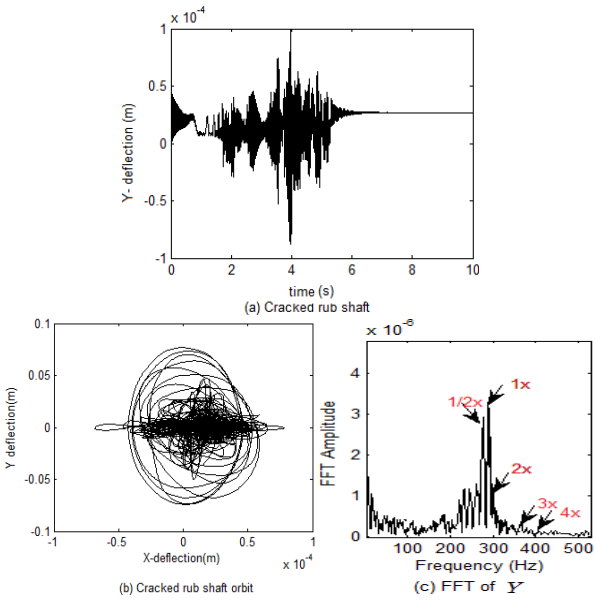

Fig. 13 Rotor system response of the lateral-rotor model without torsional flexibility, with rotor-to-stator rub, small axial force and crack, $\Delta K_\xi/K_b$=0.542, $\Delta = 2.65 \times 10^{-7}$m P=2000N.(a) Vertical cracked shaft deflection (b) Rotor response orbit, (c) Y-Lateral frequency signal

An increase in vibration amplitude was observed while the cracked rotor passed via its one-half and first critical speeds ($\omega_1 = 1917.88\, rpm$ and $\omega_2 = 3451.803\, rpm$). Rotor-stator contact increases the rotor dynamic stiffness, which in turn increases the rotor critical speed. However the presence of crack decreases the stiffness and decreases the critical speed of the rotor as seen in (Fig. 13 (a)).

Comparing the case of uncracked rotor with rub, the presence of a crack increased interactions between the rotor and stator as indicated in Fig. 13 (b). It is noted that a significant rebound appears just after the interaction and it becomes quite redundant when the stiffness of the rotor is reduced by the severity of the defects in the shaft.

In Fig. 13 (b) the orbit becomes quite disordered and the lateral motion is no longer multi-periodic. Rotor-stator rub also increased vibration level of the cracked rotor in the presence of an axial force. As a result multiple resonance peaks appear in the vibration waveform of Fig. 13 (a).

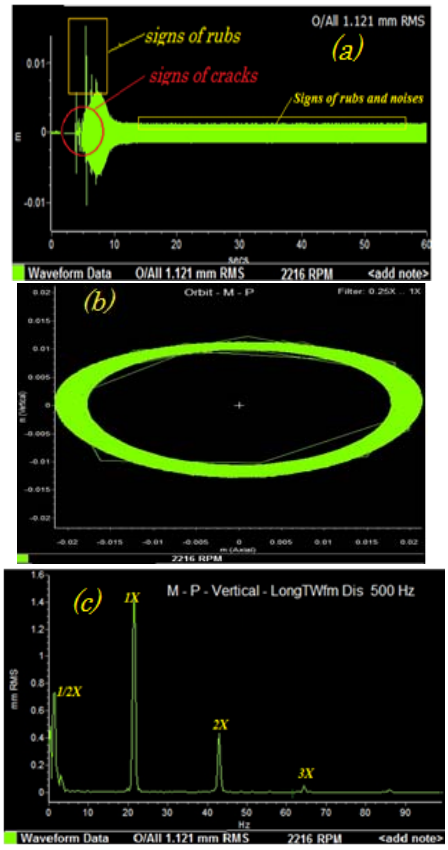

Fig. 14 Rotor system response using the lateral-rotor model at higher speed 2216 rpm with unbalance, rubbing and crack ($\Delta K_\xi/K_b$=0.5). (a) Vertical deflection (b) orbit, (b) Frequency signal domain

Approximately periodic responses of rub appear in Fig. 13 (c). Harmonics of 1× order (29.21 Hz) are noted as in results reported by [17]. The FFT spectral plot also shows that the higher frequencies, e.g., 1×, get excited by unbalance in presence of rub.

The 2×, 3× … harmonics which represent the superhamonics frequencies peaks are mainly due to crack, and harmonics at 1/2×, and 4×, etc., arise due to rotor-stator rub, and axial force. The harmonics are discernable in FFT plot (in Fig. 13 (c)).

Comparing the orbital patterns of the cracked rotor rub in Fig. 13 (a), (b), it can be concluded that, the size of the inside loop, the presence of multiple peaks of resonance and the orbital movements of the rotor passing via the first critical speed are totally different and can provide information on crack presence.

Examining the system response in the presence of a crack, peaks of successive amplitude indicating super harmonic resonance appear in Fig. 13 (c).

The size of the inside loop is drastically affected by the crack and the rub. So, the orbital changes of the rotor via one-half of the first critical speed can be used as an indicator of a transverse crack, and the bounces inside the loops can be assigned as rub signature.

The experiment on cracked rotor is performed on an unbalanced shaft with two different external forces. The first is the friction forces which are of course, a consequence of applied rubbing and the second is the crack forces, these crack forces apply simultaneously with a frictional force to the rotor motion, resulting in a fluctuation of rotor speed.

It is noticed that in the range from 1207 – 2216 rpm the rotor was running very rough during the experimental procedure with a maximum rotor frequency of 500 Hz, which made it difficult to collect the vibration measurements as they were highly irregular.

The response of cracked shaft is characterized by a main peak at the synchronous frequency of 22.5 Hz. The amplitude of these peaks evolves in a coherent manner and shows the presence of sup-harmonics. The crack and noise induced harmonics of the spin speed (2X, 3X . . .) can be seen in the response but their magnitude is very small compared to the 1X frequency component (Figs. 12 (c), 14 (c)). These harmonies show that the rotation frequency is sensitive at all frequencies for the damaged machine.

The observation of the peaks in Figs. 12 (c) and 14(c) makes it possible to materialize the shaft indices cracks under the effect of mass, rotor speed, and rubbing. The crack appears more easily detectable in both cases through the crest factor observable at the start of rotation of the shaft. The crack presence seems easier to observe through the peak factor.

At time t = 0, the crack is completely open, when the speed of rotation passes through the sub-multiples of the critical speed (22.5 Hz), examination of the vibration response of the system shows the presence of peaks successive amplitude indicating the presence of super-harmonic resonance in both Figs. 12 and 14; only the first few harmonics are significant effects on the vibration response of the system.

The presence of the crack and the friction forces result in a slight decrease in the amplitude of resonance frequencies. Thus, the first resonance frequencies of the fissured structures in Fig. 12 (b) are similar to those given in Fig. 14 (b).

As previously mentioned in Fig. 13 (c), harmonics of 1× order (22.5 Hz) are noted as in results reported in simulation. The FFT spectral plot shows that the higher frequencies, e.g., 1×, get excited by unbalance in presence of rub.

The 2×, 3× … harmonics which represent the sup-harmonics frequencies peaks are mainly due to crack, and harmonics at 1/2×, etc., arise due to rotor-stator rub. These harmonics are clearly seen in FFT plot (Figs. 12 (c) and 14 (c).

Analysis of Fig. 14 reveals that cracking has a big effect on the rotor response than rubbing as the amplitude of vibration is largely attenuated in comparison to the case of crack with no rub vibrations. Once again the experiment results revealed like observed in simulation (Fig. 13) that the effect of rubbing on the waveform in presence of crack is less significant and also that, the critical speed of the rotor decreases due to the breathing of the crack.

As can be seen in Fig. 14 when the cracked-rubbing shaft is spinning away from critical speed, the vibration waveform is not greatly affected by rubbing. However, when the cracked-rubbing shaft speed is close to its critical speed (2216 rpm), the vibration amplitude is increased and the waveform is obviously distorted as a result of the breathing and severe rubbing contact.

The analysis of orbits shows that for cracked rotors, the orbit described by the rotor is formed of $\boldsymbol{n}$ interlaced loops, and the level of the first harmonic is dominant Fig. 12 (c). For a given combination crack contacts, rotor to stator, the dynamic system is the seat of resonances sub-critical and super-harmonics (Fig. 14 (c)).

The review of the vibration response of the dynamic system again shows that, the orbit of the rotor is formed of $\boldsymbol{n}$ non-regular loops interlaced (Fig. 14 (a)). One more time the presence of the crack is dominant compared to the contact of the rotor effects.

The agreement between theory and experiment can be observed when comparing the waveform of computed values with diagrams of experimental tests.

Thus, as predicted before, recording sub-harmonics and super-harmonic resonances through the critical speed, the presence of multiple peaks and the change of the shape of the orbit (number of loops) can be a good indicator of the existence of contact and cracks in a rotor.

XVI. Rotor-Stator-Rub and Crack in 4 D.O.F

The torsional-lateral vibrations of unbalanced rotor-stator with rub and a transverse crack and axial force are theoretically investigated using (12). Parametric resonance is expected to occur in an axially loaded shaft when the exciting frequency exceeds the shaft bending natural frequency ω_B [4]. Torsional resonance occurs when the angular velocity of the rotating shaft equals the torsional natural frequency ω_T.

Simulation of rotor response using torsional lateral-rotor model is made under fourth hypothesis.

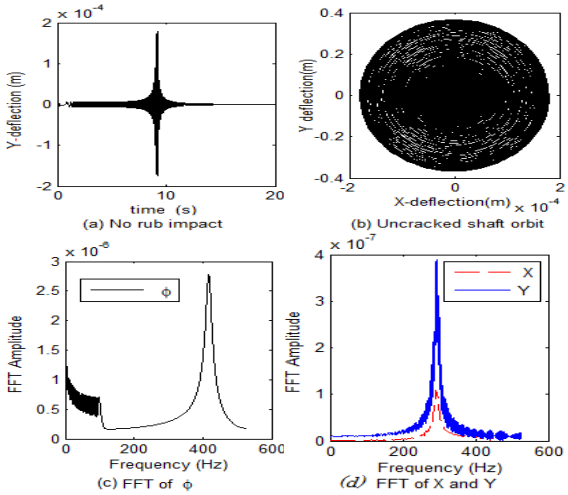

Fig. 15 Dynamics system response from lateral-torsional-rotor model, no rub, no crack $\Delta K_\xi/K_b$=0. P=2000N, $\psi \neq 0$, $\omega_T = \omega_L$ (a) Vertical shaft deflection (b) Rotor response orbit (c) Torsional frequency signal (d) Lateral and frequency signal

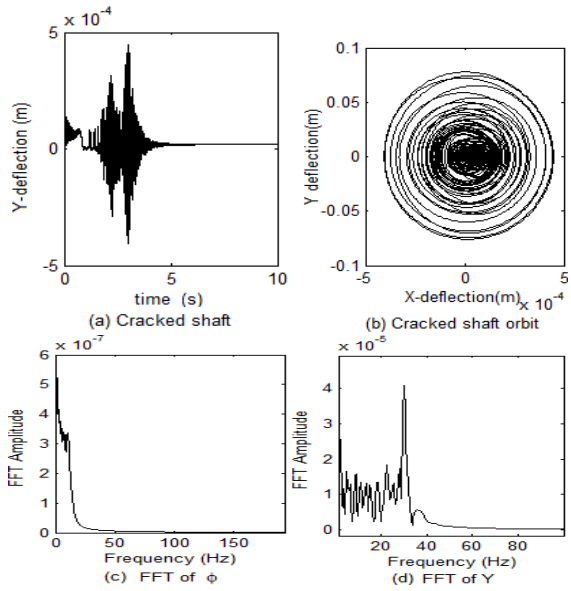

Fig. 16 Dynamics system response using the lateral-torsional rotor model, no rub, $\Delta K_\xi/K_b$=0.542, P=2kN, $\psi \neq 0$;$\omega_T = \omega_L$ (a) Vertical shaft deflection (b) Rotor response orbit (c) Torsional frequency signal (d) Lateral and frequency signal

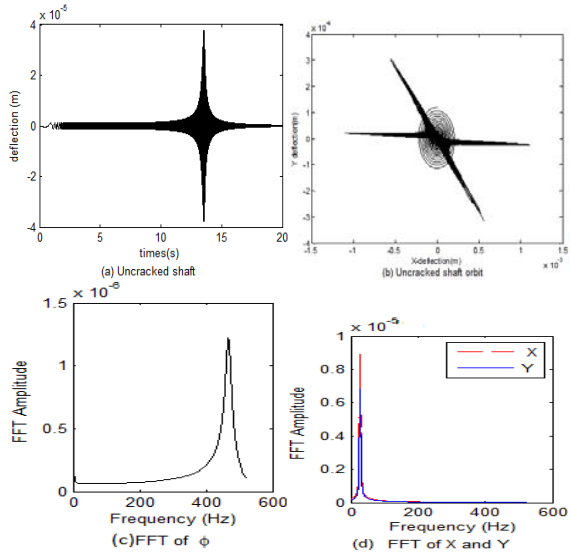

Fig. 17 Dynamics response, with rotor-to-stator-rub and axial force but no crack $\Delta K_\xi/K_b$=0. P=2000N, $\Delta = 2.65 \times 10^{-7}$m, (a) Vertical cracked shaft deflection (b) Rotor response orbit, (c) Torsional frequency signal domain, (d) Lateral frequency signal domain

For the first hypothesis the system response is simulated when the axial force is exerted and without rub. The torsional and lateral natural frequencies are then equal, $\omega_T = \omega_L$. And in the second hypothesis rotor is operated only in the presence of a crack and an axial force.

The third and fourth is considering both rub-crack effect for which the torsional resonance behavior occur when $\omega_T \gg \omega_L$.

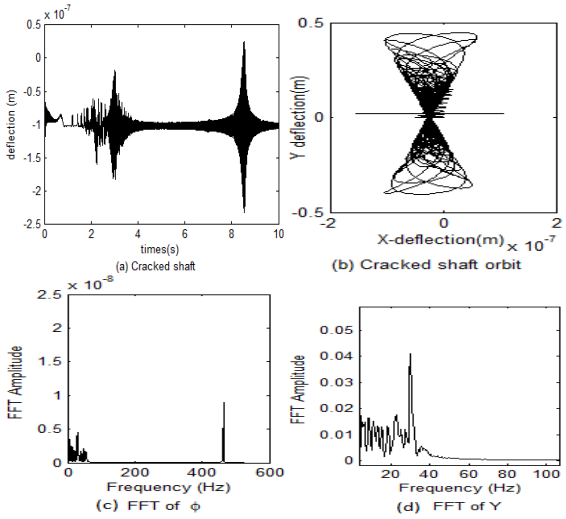

Fig. 18 System response with, rub-crack, axial force: $\Delta K_\xi/K_b$=0.542. P=2000N,$\omega_T \gg \omega_L$,$\Delta = 2.65 \times 10^{-7}$m, (a) Vertical cracked shaft deflection (b) Rotor orbit response (c) Torsional frequency signal (d) Lateral frequency signal

Fig. 15 (a) shows the synchronous rotor lateral response as a function of time. The shaft attains critical speed at 2042, 4 rpm indicated by peak amplitude in Figs. 15 (d) and 16 (d). The variation in FFT amplitude with frequency is plotted in Figs. 15 (c) and 16 (d).

As noted in Figs. 15 (c), 15 (d), 17 (c) and 17 (d) once the critical speed is traversed, the amplitude of vibration decreases. This indicates that only unbalance and axial force are the source of the above vibrations.

Spectral plots of the signal in Figs. 16 (d) and 14 (d) show an increase in the magnitude of frequency components before resonance; while it indicates a reduction in the magnitude of the second harmonic and a disappearance of higher frequency components. Fig. 17 (b) shows an elliptical orbit due to model anisotropy and shows also the second rigid mode shapes of the modeled rotor. Presence of the second rigid mode is attributed to multiple factors; higher axial force, the transient vibration, which follows the removal of the friction torque in the rub free zone and the presence of the flexibility of the cracked shaft.

The orbit presented in Fig. 17 (b) revealed as noted in [4], that the direction of the two maximum responses changes due to anisotropy model of rotor. Unlike the orbit of the cracked rotor, it describes deflection shape of the system due to vibration and to local flexibility of the rotor at the damage location.

Figs. 16 (a) and 18 (a) are waveforms registered respectively at a rotational speed of 2309.4 rpm and 4510.21 rpm. Two high resonance points and three resonance points developed from the excitation between the torsional and lateral rotor. The first one is the ordinary resonance and the other two are situated at the median and high resonance in Fig. 18 (a). Therefore, the frequency spectrum (Fig. 18 (d)) contains a vibration component corresponding to these modified processional speeds.

In Fig. 18, it evident that axial force, crack and rub force conspicuously affects the vibration response in comparison to the case of no rub-crack vibrations in Fig. 15.

Examining the maximum power spectral density and shaft trajectory of a cracked rotor, an increase in the spectral power density at half the critical speed can be used to diagnose presence of a breathing transverse crack.

XVII. Conclusion

The experiment-analytic study on torsional-lateral vibrations of unbalanced cracked rotor-stator system revealed that:

1. The shaft precessing orbits are largely distorted due to severe rubbing and highly stretched due to the breathing crack. The orbits patterns are major parameters to diagnose rubbing rotors.
2. Spectral analysis has indicated that crack onset may best be examined by observing super harmonics. The 2×, 3× … harmonics which represent the sup-harmonics frequencies peaks are mainly due to crack, and harmonics at 1/2×, etc., arise due to rotor-stator rub.
3. It appears also that experimentally the absence of axial force effect did not disrupt the waveform signal, its effect on the vibration response of the rotor in the presence of a crack is considerable for a large axial force.
4. The experimental results compared with those obtained by simulation have revealed similarity. Indeed, as mentioned above, the elliptic shape orbits, the frequency analysis show similar parameters at the same time by simulation and experiment.

Acknowledgment

Support by the Department of Mechanical Engineering, VUT towards this work is highly acknowledged by the authors.

References

[1] T. H. Patel, and A. K. Darpe, Coupled bending torsional vibration analysis of rotor with rub and crack, Journal of Sound and Vibration Vol. 326, 2009, pp 740–752.

[2] F. Chu, and W. Lu, Determination of the rubbing location in a multi-disc rotor system by means of dynamic stiffness identification. Journal of sound and vibration, 2001. 235-246.

[3] R. F. Beatty, Differentiating Rotor response due to radial rubbing, Journal of Vibration, Acoustics, Stress, and Reliability in Design Vol107, 1985, pp151–160.

[4] B. O. Al-bedoor, Transient torsional and lateral vibrations of unbalanced rotors with rotor-to-stator rubbing. Journal of Sound and vibration 229(3), 2000, 627-645.

[5] J. T. Sawicki, J. Padovan, and R. Al-Khatib, The Dynamics of Rotor with Rubbing. International Journal of Rotating Machinery 1999, Vol. 5, No. 4, 1998, pp. 295-304.

[6] J. T. Sawicki, X. Wu, G. Y. Baaklini, and A. L. Gyekenyesi, "Vibration-based crack diagnosis in rotating shafts during acceleration through resonance," in Nondestructive Evaluation and Health Monitoring of Aerospace Materials and Composites II, vol. 5046 of Proceedings of SPIE, 2003, pp. 1–10, San Diego, Calif, USA.

[7] Y. B. Kim, and S. T. Noah, Bifurcation analysis for modified Jeffcott rotor with bearing clearances, Nonlinear Dynamics Vol. 1, 1990, pp 221-241.

[8] F. Chu, and W. Lu, Stiffening effect of the rotor during the rotor-to-stator rub in a rotating machine, Journal of Sound and Vibration Vol. 308, 2007, pp 758–766.

[9] R. Sukkar, and A. S. Yigit, Analysis of fully coupled torsional and lateral vibrations of unbalanced rotors subject to axial loads. Kuwait J. Sci. Eng. 35 (2B), 2008, pp. 143-170.

[10] R. Gasch, A Survey of the Dynamic Behaviour of a Simple Rotating Shaft with Transverse Crack, *Journal of Sound and Vibration*, 1993, 160(2): 313-332.

[11] B. Grabowski, The vibrational behavior of a turbine rotor containing a transverse crack. *ASME Design Engineering Technology Conference, St. Louis*, 1979. Paper No. 79-DET-67.

[12] J. J. Sinou, Condition Monitoring for Notched Rotors Through Transient Signals and Wavelet Transform Experimental Mechanics 49 (2012) 683-695.

[13] I. Mayes, and W. Davies, The vibration behavior of a rotating shaft system containing a transverse crack. Vibration in rotating machinery, Inst. Mech, E. 1976, p.53-65.

[14] B. X. Tchomeni, A. A. Alugongo, and L. M. Masu, In situ Modelling of Lateral-Torsional Vibration of a Rotor-Stator with Multiple Parametric Excitations. World Academy of Science, Engineering and Technology International Journal of Mechanical, Aerospace, Industrial and Mechatronics Engineering Vol:8 No:11, 2014.

[15] A. S. Yigit, and A. P. Christoforou, Coupled Torsional and Bending Vibrations of Actively Controlled Drillstings. Journal of Sound and Vibration, 2000, 234: 67-83.

[16] A, D. Dimarogonas, Vibration Engineering, West Publishers, St. Paul. 1976.

[17] A. K. Darpe, Dynamics of cracked rotor. PhD Thesis, IIT Delhi, 2000.